Field-effect Ion-transport Devices with Carbon Nanotube Channels: Schematics and Simulations

Oh Kuen Kwon*, Jun Sik Kwon*, Ho Jung Hwang** and Jeong Won Kang**
* SeMyungUniversity, Jecheon, Chungbuk 390-711, Korea
Tel : +82-043-649-1487 Fax : +82-043-649-1740 E-mail: kok1027@semyung.ac.kr
** Dept of Electronic Engineering, Chung-ang University, Seoul, 156-756, Korea
Tel : +82-02-820-5296 Fax : +82-02-812-5313 E-mail: gardenriver@korea.com

Abstract: We investigated field-effect ion-transport devices based on carbon nanotubes by using classical molecular dynamics simulations under applied external force fields, and we present model schematics that can be applied to the nanoscale data storage devices and unipolar ionic field-effect transistors. As the applied external force field is increased, potassium ions rapidly flow through the nanochannel. Under low external force fields, thermal fluctuations of the nanochannels affect tunneling of the potassium ions whereas the effects of thermal fluctuations are negligible under high external force fields. Since the electric current conductivity increases when potassium ions are inserted into fullerenes or carbon nanotubes, the field effect due to the gate, which can modify the position of the potassium ions, changes the tunneling current between the drain and the source.

Ex. Ionic field-effect memory and transistor, Carbon nanotube, Nanochannel

1. INTRODUCTION

Ion transport in nanochannels due to external electric fields can significantly modify the surface charge density of the nanochannels, the ion concentration, and the ionic current. Therefore, ion and molecule transports in nanoscale channels have recently received increasing attention [1]. Rafii-Tabar [1] reviewed recent computational modeling of the transport properties inside carbon nanotubes. Daiguji *et al.* [2] investigated theoretical modeling of the ionic distribution and transport in nanofluidic channels using silica nanotubes, 30 nm in diameter and 5 μm long. Using molecular dynamics (MD) simulations, Chan *et al.* [3] investigated ion transport in simple nanopores, Hanasaki *et al.* [4] investigated Ar or He flow inside carbon nanotube (CNT) junction as a molecular nozzle and diffuser, Joseph *et al.* [5] investigated ionic transport in CNTs for ion-channel-based biosensors, and Tuzun *et al.* [6,7] investigated the fluid flow of C_{60}, He, or Ne inside CNTs. Thus, nanospaces or nanochannels inside CNTs have also opened new applications as storage materials and fluid flow channels with high capacity and stability.

It is anticipated that systems based on ion transport in nanochannels can be applied to nanoscale data storage devices [8] and unipolar ionic field-effect transistors [2]. After the investigation of bucky shuttle memory elements by Kwon *et al.* [9], using classical MD simulations under electrostatic force fields, various molecule shuttle devices have been investigated: the metallofullerene shuttle memory element in carbon nanocapsules [10], the bucky shuttle three-terminal switching device [11], and memory devices based on carbon peapods [12] and boron-nitride peapods [13]. Also, the structural and the electrical properties of alkali-metal-doped CNTs have been investigated by Jeong *et al.* [14,15] who attempted both experimental and theoretical investigations of cesium ions encapsulated in single-walled CNTs.

For the bucky shuttle memory of Kwon *et al.* [9], the stored data can be measured by using the current pulse in the connecting wires; that current is caused by the motions of charged molecules or ions due to the applied probing voltage. Therefore, if the stored data is to be read, the $K^+@C_{60}$ or ions should be shuttled. For example, when the $K^+@C_{60}$ settles in the position of 'bit 1', the $K^+@C_{60}$ has to move toward the position of 'bit 0' during the data reading processes; then, 'bit 1' can be measured. After the data has been read, the $K^+@C_{60}$ should be returned to the position of 'bit 1' to maintain its original data. Therefore, data reading processes have to include data erasing/writing processes, so both the power consumption and the data processing time will increase.

For the bucky shuttle memory device of Kwon *et al.*, a decrease in the electric field is clearly achieved from the field-screening effect of the outer capsule; then, the penetrating field also partially acts on the *endo* metallic ions because of the field-screening effect of the C_{60} fullerene. CNTs with hemisphere caps can act as Faraday cages or cups, screening the field from the trapped nanotube. Delaney and Greer [16] found that the C_{60} acted effectively as a small Faraday cage, with only 25% of the field penetrating the interior of the C_{60}. They also predicted that the field penetration would increase with the fullerene radius. Therefore, the CNT with both side caps in this work is a semiconductor. Although the endohedral ions are partially shielded from external electrical fields due to the hemisphere cap acting as a Faraday cage, the penetrating field can act on the endohedral ions. Therefore, the final electric field acting on the *endo* metallic ion is as low as 0.0625 of the applied external field. However, for the ion shuttle device in this work, the electric field acting on the encapsulated ions is 0.25 of the applied external field. The force acting on the encapsulated ion is higher than that acting on the

C_{60} fullerene. The mass of encapsulated ion (such as Li, Na, and K) is lower than the mass of C_{60} fullerene. Since the binding energy of the encapsulated ion in the CNT is lower than that of C_{60} fullerene in the CNT, the encapsulated ions are easily accelerated. Therefore, ion shuttle devices are more effective than *endo*-fullerene shuttle devices in the viewpoint of operating speed and power consumption.

In this work, we consider potassium ions as the encapsulated ions because potassium atoms are a low-mass impurity and are fully ionized when they are intercalated between graphite plates or into CNTs [17-19]. Also the electronic properties of the CNTs are modified with the intercalation of potassium ions; then, the electric current conductivity increases when the potassium ions are inserted into fullerene [20-22] or CNT [23]. In some cases, fullerenes and CNTs with intercalated potassium ions have shown superconductivity [20-22]. However, since the potassium ions easily diffuse in the CNTs due to the low binding energy of the potassium ion in the CNT, the energetic or structural barriers that prohibit the potassium ions from diffusing in the CNT should be considered for ion shuttle memory devices. This can be achieved for a nanochannel that prohibits the potassium ions from diffusing in the CNT.

In this paper, we investigate potassium ion transport through a (5, 5) CNT as a nanochannel by using classical MD simulations under applied external force fields. We present controllable potassium ion transport in (5, 5) CNT by using the MD simulations. We also show model schematics that can be applied to nanoscale data storage devices and unipolar ionic field-effect transistors.

2. METODS

For carbon–carbon interactions, we used the Tersoff-Brenner potential function [24-26] that has been widely applied to carbon systems. For the potassium–potassium and the potassium–carbon interactions, we employed the force-field method developed and used by Goddard and co-authors for studying potassium-intercalated fullerenes [17-19]. They assumed that the potassium is fully ionized to K^+ and that the charges are distributed uniformly on the single-walled CNT. This assumption is consistent with the assumptions used in the derivation of the van der Waals parameter for $K^+ - K^+$ and $C - K^+$; then, the force-field method by Goddard and co-authors give accurate results for the lattice parameter and other properties for potassium-intercalated graphite compounds. Since the binding energies between K atoms or . ions are very low, the potassium ions moved as individual particles when the potassium ions are accelerated under an external force field. Partially ionized potassium clusters can be achieved in endohedral potassium clusters encaged in a nanocapsule [27]. However, the MD simulations in our previous work showed that each potassium atom moved as an individual particle when external force fields were applied [8]. Individual potassium ions can be fully ionized in CNTs. Therefore, during the MD simulations, we assumed that the potassium atoms encapsulated in the CNT were fully ionized under the external force fields [8].

We used both steepest descent (SD) and MD methods. The MD simulations used the same MD methods as were used in our previous works [28-32]. The MD code used the velocity Verlet algorithm and neighbor lists to improve computing performance [33]. The MD time step was 5×10^{-4} ps. Initial velocities were assigned from the Maxwell distribution, and the magnitudes were adjusted so as to maintain the temperature in the system constant. A Gunsteren-Berendsen thermostat was used to control the temperature for all carbon atoms but not for potassium ions [33].

Figure 1(d) shows the structure used in this work. The nanochannel is a (5, 5) CNT that is seamlessly connected with both side cages. When a semiconducting CNT is used as the nanochannel instead of a metallic CNT, the field intensity in the semiconducting CNT is slightly lower than that in the metallic CNT. Therefore, field-effect ion transport can be effectively achieved when a metallic CNT is used as a nanochannel. The cages are extended C_{240} fullerenes, truncated icosahedral cages. The bandgap of the C_{240} fullerene used as the cage in this work is 1.241072 eV [34]. As the radii and the lengths of the fullerenes and the nanocages increase, since their bandgaps are decreased [34,35], the bandgap of the nanocage used in this work is lower than that of the C_{240} fullerene. The length of the system along the tube axis (z-axis) is 80 Å. The numbers of encapsulated potassium ions used are 3 to 13. The initial structure was relaxed by using the SD method. We performed the MD simulation for the encapsulated potassium ions at various values of the temperature and the external force field.

3. RESULTS AND DISCUSSION

When the external force field was not applied to the system, the trajectories of 13 potassium ions along the z-axis are shown for 100, 300, and 500 Kin Fig. 1(a)-1(c), respectively. Figure 1(d) shows the atomic structures for the same temperatures at 200 ps. When the 13 potassium ions were encapsulated in the bottom cage, the potassium ions diffused through the nanochannel toward the other side cage. As the temperature was increased, since the thermal fluctuation of the nanocahnnel increased, the rate of the ion injection into the nanochannel slightly increased; and then, the injected ions easily moved toward the other side without disturbance. Therefore, a few ions remained in nanochannel whereas most of ions remained in the two nanocages. As the temperature was decreased, the potassium ions injected into the nanochannel were almost uniformly distributed in the nanochannel because of low diffusivity of the potassium ions in the nanochannel. Therefore, when bit classification is achieved by position detection of the encapsulated potassium ions, such as in previous works [8], we anticipate that data storage in nanochannel devices, as shown in Fig. 1, can be achieved from position control of the encapsulated potassium ions by the external force fields.

We performed the MD simulations as functions of the number of the potassium ions, the external force field, and the temperature. The external force fields were 0.005 to 0.02 V/Å and the temperatures were 100, 300 and 500 K. Positive force fields were applied from 0 to 100 ps, and the negative force fields were applied from 100 to 200 ps. Figure 2 shows the trajectories of 13 potassium ions under applied external force fields at 300 K. As the applied external force field was increased, the potassium ions rapidly went through the nanochannel. Under low external force fields, thermal fluctuations of the nanochannel affected the tunneling of potassium ions whereas the effects of thermal fluctuations were negligible under high external force fields. Figure 2(d) shows the atomic structures at 99.5 and 199.9 ps under an external force field of 0.02 V/Å. For the case of 0.005 V/Å, not all potassium ions go through the nanochannel. For the case of 0.02 V/Å, all potassium ions go through the nanochannel. Therefore, for data storage devices based on ion transport in a nanochannel, a high speed bit-flop can be achieved with a high force field under the condition that the high field cannot break the atomic bonds of the CNT. However, a switching device can operate when only a few ions transport through the nanochannel. This will be discussed with Fig. 4.

Figure 3(a) shows the mean position of the 13 potassium ions as a function of the MD time for the MD simulation of 13 potassium ions under 0.02 V/Å. We can see that all ions were transported during 30 ps. Therefore, for the cases investigated in this work, the bit-flop speed should be above 30 ps; then, the maximum switching frequency will be below 33 GHz for a data storage device. Figure 3(b) shows the distributions of the number of ions along the tube axis for various MD times. In the condition that all encapsulated potassium atoms are fully ionized, as discussed in Section II, we can consider these distributions to be the same as the surface charges of the nanotube along the axis of the nanochannel. As the MD time increases to 20 ps, the number of ions encapsulated in the bottom cage decreases whereas the number of ions encapsulated in the upper cage increases because of ion transport from the bottom to the upper cage. At 31 ps, all ions are transported.

For the bucky shuttle memory of Kown *et al.* [9], the stored data can be measured by using the current pulse in the connecting wires; this current is caused by the motions of the charged molecules or ions due to the applied probing voltage. Therefore, if the stored data is to be read, the $K^+@C_{60}$ or ions should be shuttled. For example, when the $K^+@C_{60}$ settles in the position of 'bit 1', the $K^+@C_{60}$ should be moved toward the position of 'bit 0' during the data reading processes; then, 'bit 1' can be measured. After the data is read, the $K^+@C_{60}$ should be returned to the position of 'bit 1' to maintain its original data. Therefore, the data reading processes have to include data erasing/writing processes, so both the power consumption and the data processing time will increase. The bit classifications by this method are very complicated to define and to detect by using connected electrodes. Another methodology for bit classification can be achieved from the direction of the applied force fields. For bit writing/erasing, a high external force field is applied; when all ions transport the nanochannel, the positions of the ions can be maintained in the cage by a weak external force field. Therefore, bit can be classified with the direction of the weak applied force field. By this method, data reading processes need not include the data erasing/writing processes suggested by Kwon *et al.* [9]. The data reading speed with the second method is higher than that with the previous method [9] whereas electric power is continually consumed because a weak field should be continually applied to maintain the bit. If diffusion of ions through the nanochannel does not occur, bit classification can be achieved from the electric field induced by the surface charge distributions, as shown in Fig. 3(b). However, for the system investiaged in this work, thermal diffusion of ions through the nanochannel was found, as shown in Fig. 1.

Another schematic of a data storage device is shown in Fig. 4. In this method, the stored data can be detected by the positions of the ions as with the previous method of Kwon *et al.* [9] whereas to read the stored data, there is no ion transport through the nanochannel. The data are detected by using the drain-source current (i_{ds}). The electronic properties of the CNTs are modified by the intercalation of potassium ions; then, the electric current conductivity increases when the potassium ions are inserted into the fullerene [20-22] or the CNT [23]. In some cases, fullerenes and CNTs with intercalated potassium ions have shown superconductivity [20-22]. The bandgap of the C_{240} fullerene is 1.241072 eV [34]. As the number of carbon atoms composed of fullerenes and the length of the carbon nanocages increase, since their bandgaps are decreased [34,35], the bandgap of the nanocage used in this work must be considerably lower than that of the C_{240} fullerene. For the fullerene intercalated with potassium, the density of states at the Fermi level is observed to increase and the electron-hole pair excitations also increases [22]. Therefore, when the potassium ions stay between the drain and the source, the current i_{ds} is $I_{\text{turn-on}}$, as shown in Fig. 4(a) whereas when there are no ions between the drain and the source, the current i_{ds} is $I_{\text{turn-off}}$ as shown in Fig. 4(b). From previous works [20-23], $I_{\text{turn-on}}$ is clearly higher than $I_{\text{turn-off}}$.

The device in Figs. 4(a) and 4(b) can be used a nanoscale ionic field-effect transistor [2]. When the potassium ions are controlled by the bias of the gate, this device can be used as a three-terminal switching device. Both sides of the right-hand cage are connected to the drain and the source electrodes. Therefore, the right-hand cage is the current tunneling channel. Since the field effect by the gate can modify the tunneling current (i_{ds}) between the drain and the source, this device is very similar to the field-effect transistors that have been widely applied to the contemporary electronic memory and switching

devices. The turn-on state of the device can be achieved when some ions partially transport to the cage between the drain and the source. However, the turn-off state of the device should be achieved when no ion remains inside the cage between the drain and the source. Figure 4(c) shows simple voltage-current schematics for the operation of the ionic field-effect transistor. When the potential drop (V_{DS}) between the drain and the source is always positive, the tunneling current (i_{ds}) between the drain and the source changes with the gate bais. When the gate bias is in the turn-on state for the ionic field-effect transistor ($V_{turn\text{-}on}$), i_{ds} becomes $I_{turn\text{-}on}$ with a time delay of t_d. The time delay t_d is almost ~30 ps when the gate bias V_g is 1.6 V, as shown in Figs. 2 and 3 in this work. When the gate bias is in the turn-off state for the ionic field-effect transistor ($V_{turn\text{-}off}$), i_{ds} becomes $I_{turn\text{-}off}$ with a time delay of t_d. We anticipate that unipolar ionic field-effect transistors can be realized with several nanotechnologies.

4. SUMMARY

A field-effect ion-transport device based on carbon nanotubes has been investigated by using classical molecular dynamics simulations under applied external force fields. We found controllable potassium ion transport in the (5, 5) carbon nanotube and presented a model schematics that could be applied to a nanoscale data storage device and a unipolar ionic field-effect transistor. When the applied external force field is increased, the potassium ions rapidly go through the nanochannel. Under low external force fields, thermal fluctuations of the nanochannel affect the tunneling of the potassium ions whereas the effects of thermal fluctuations are negligible under high external force fields. We proposed several data reading methods and then showed model schematics for a nanoscale ionic field-effect memory and transistor. The electronic properties of the carbon nanotubes are modified with the intercalation of potassium ions, and the electric current conductivity increases when potassium ions are inserted into fullerenes or carbon nanotubes. Since the field effect due to the gate can modify the tunneling current between the drain and the source, this device is very similar to the field-effect transistors that have been widely applied to the contemporary electronic memory and switching devices.

References

[1] H. Rafii-Tabar, Phys. Rep. **390**, 235 (2004).

[2] H. Daiguji, P. Yang and A. Majumdar, Nano Lett. **4**, 137 (2004).

[3] K-Y. Chan, Y. W. Tang and I. Szalai, Mol. Simul. **30**, 81 (2004).

[4] I. Hanasaki, A. Nakatani and H. Kitagawa, Sci. Tech. Adv. Mater. **5**, 107 (2004).

[5] S. Joseph, R. J. Mashl, E. Jacobsson and N. R. Aluru, Nano Fluidics and Transport in Technical Proceedings of the 2003 Nanotechnology Conference and Trade Show, Vol. 1, Chap. 8 pp. 158-161 (2003).

[6] R. E. Tuzun, D. W. Noid, B. G. Sumpter and R. C. Merkle, Nanotechnology **7**, 241 (1996).

[7] R. E. Tuzun, D. W. Noid, B. G. Sumpter and R. C. Merkle, Nanotechnology **8**, 112 (1997).

[8] J. W. Kang and H. J. Hwang, J. Korean Phys. Soc. **44**, 879 (2004).

[9] Y. K. Kwon, D. Tomanek and S. Iijima, Phys. Rev. Lett. **82**, 1470 (1999).

[10] J. W. Kang and H. J. Hwang, J. Phys. Soc. Japan **73**, 1077 (2004).

[11] H. J. Hwang and J. W. Kang, Physica E **23**, 35 (2004)

[12] J. W. Kang and H. J. Hwang, Jpn. J. Appl. Phys. **73** (7A), 4447(2004).

[13] W. Y. Choi, J. W. Kang and H. J. Hwang, Physica E **23**, 135 (2004).

[14] G. H. Jeong, A. A. Farajian, T. Hirata, R. Hatakeyama, K. Tohji, T. M. Briere, H. Mizuseki and Y. Kawazoe, Thin Solid Films **435**, 308 (2003).

[15] G. H. Jeong, A. A. Farajian, R. Hatakeyama, T. Hirata, T. Yaguchi, K. Tohji, H. Mizuseki and Y. Kawazoe, Phys. Rev. B **68**, 075410 (2003).

[16] P. Delaney and J. C. Greer, Appl. Phys. Lett. **84**, 431 (2004).

[17] G. Gao, T. Cagin and W. A. Goddard III, Phys. Rev. Lett. **80**, 5556 (1998).

[18] G. Chen, Y. Guo, N. Karasawa and W. A. Goddard III, Phys. Rev. B **48**, 13959 (1993).

[19] Y. Guo, N. Karasawa and W. A. Goddard III, Nature **351**, 464 (1991).

[20] R. S. Lee, H. J. Kim, J. E. Fischer, A. Thess and R. E. Smalley, Nature **388**, 255 (1997).

[21] A. M. Rao, P. C. Eklund, S. Bandow, A. Thess and R. E. Smalley, Nature **388**, 257 (1997).

[22] M. Montalti, S. Krishnamurthy, Y. Chao, Yu. V. Butenko, V. L. Kuznetsov, V. R. Dhanak, M. R. C. Hunt and L. Siller, Phys. Rev. B **67**, 113401 (2003).

[23] M-H. Du and H-P. Cheng, Phys. Rev. B **68**, 113402 (2003).

[24] J. Tersoff, Phys. Rev. B **38**, 9902 (1988).

[25] J. Tersoff, Phys. Rev. B **39**, 5566 (1989).

[26] D. W. Brenner, Phys. Rev. B **42**, 9458 (1990).

[27] J. M. Cabrera-Trujillo, J. A. Alonso, M. P. Iniguez, M. J. Lopez and A. Rubio, Phys. Rev. B **53**, 16059 (1996).

[28] J. W. Kang and H. J. Hwang, Nanotechnology **13**, 524 (2002).

[29] J. W. Kang and H. J. Hwang, Physica E **15**, 82 (2002).

[30] J. W. Kang and H. J. Hwang. J. Phys.: Condens. Matter **14**, 2629 (2002).

[31] J. W. Kang and H.J. Hwang. J. Korean Phys. Soc. **43**, 1139 (2003).

[32] J. W. Kang and H. J. Hwang, J. Korean Phys. Soc. **40**, 946 (2002).

[33] M. P. Allen and D. J. Tildesley, *Computer Simulation of Liquids* (Oxford, Clarendon, 1987).

[34] Y-L. Lin and F Nori, Phys. Rev. B **49**, 5020 (1994).

[35] J. Cioslowski, N. Rao, and D. Moncrieff, J. Am. Chem. Soc. **124**, 8485 (2002).

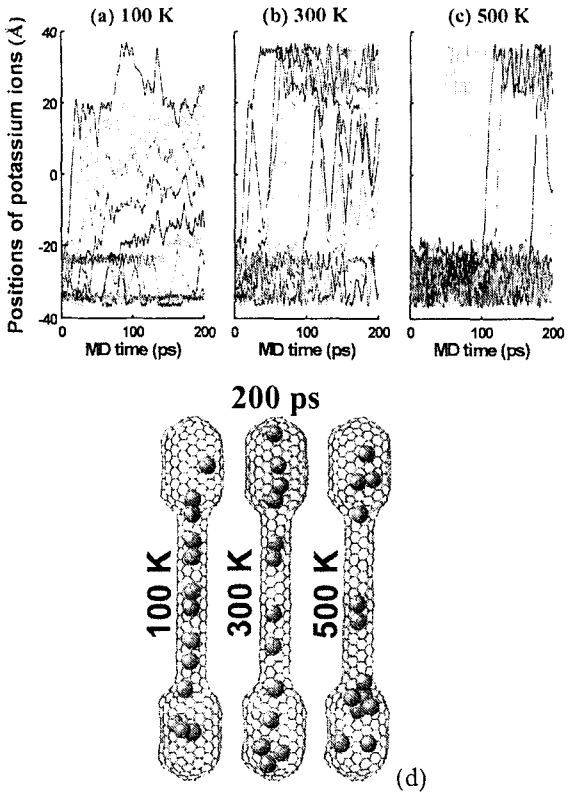

Fig. 1. (a)-(c) show the trajectories of 13 potassium ions along the z-axis at temperatures of 100, 300, and 500 K without external force fields, respectively. (d) Atomic structures with temperatures at 200 ps.

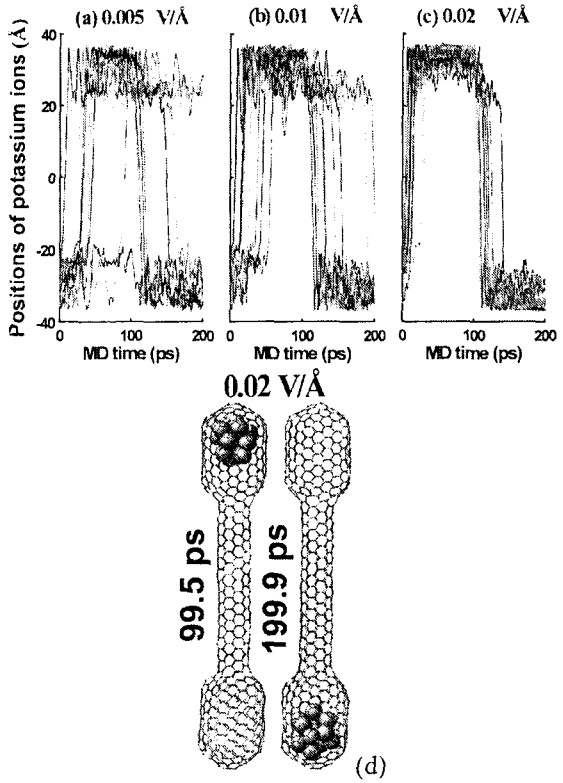

Fig. 2. (a)-(c) show the trajectories of 13 potassium ions under the applied external force fields of 0.005, 0.01, and 0.02 V/Å by using MD simulations at 300 K. (d) Atomic structures for an applied force field of 0.02 V/Å at 99.5 and 199.9 ps.

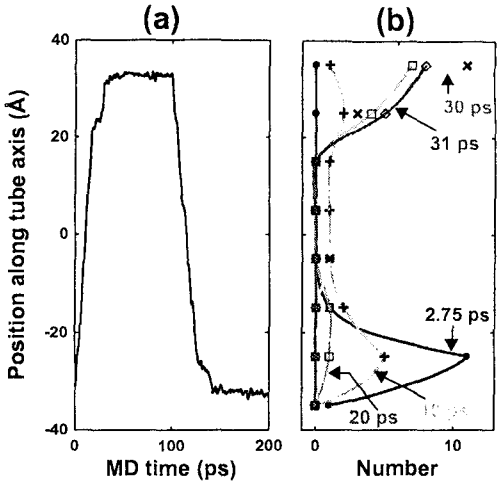

Fig. 3. (a) Mean position of the 13 potassium ions as a function of the MD time for the MD simulation of 13 potassium ions under 0.02 V/Å. (b) Distributions of the number of ions along the tube axis for various MD times.

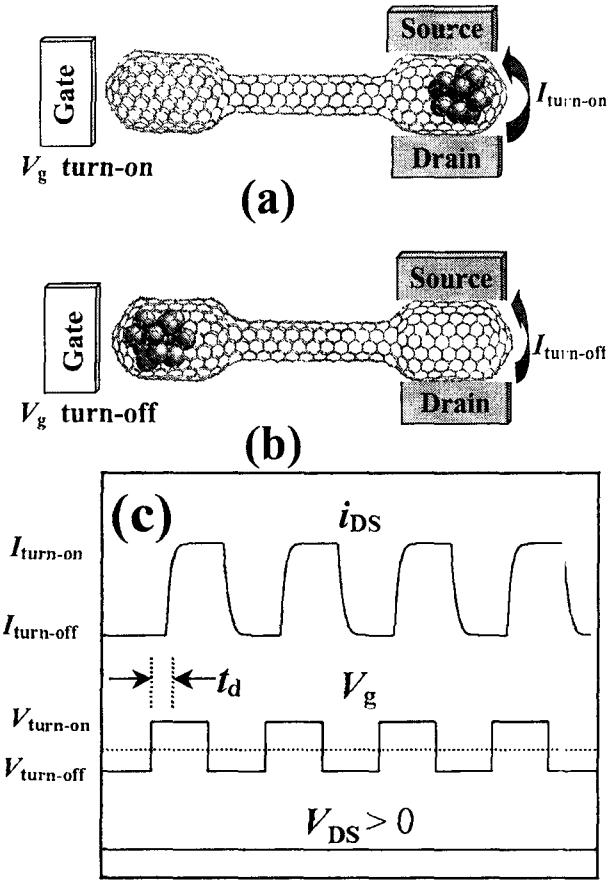

Fig. 4. Device schematics that can be used as a nanoscale ionic field-effect memory and transistor: (a) turn-on state and (b) turn-off state. (c) Simple voltage-current schematics for the operation of the ionic field-effect transistor. The potential drop (V_{DS}) between the drain and the source is always positive, and the tunneling current (i_{ds}) between the drain and the source changes with the gate bias. When the gate bias is in the turn-on state for the ionic field-effect transistor ($V_{turn-on}$), i_{ds} becomes $I_{turn-on}$ with a time delay of t_d. When the gate bias is in the turn-off state for the ionic field-effect transistor ($V_{turn-off}$), i_{ds} becomes $I_{turn-off}$ with a time delay of t_d.